Computational Materials Science 79 (2013) 736–744

Contents lists available at ScienceDirect

Computational Materials Science

journal homepage: www.elsevier.com/locate/commatsci

Effect of defects on the local shell buckling and post-buckling behavior of single and multi-walled carbon nanotubes

Mehdi Eftekhari [a], Soheil Mohammadi [b,*], Amir Reza Khoei [c]

[a] Department of Civil Engineering, Science and Research Branch, Islamic Azad University, Tehran, Iran
[b] High Performance Computing Lab, School of Civil Engineering, University of Tehran, Tehran, Iran
[c] Center of Excellence in Structures and Earthquake Engineering, Department of Civil Engineering, Sharif University of Technology, Tehran, Iran

ARTICLE INFO

Article history:
Received 17 February 2013
Received in revised form 30 June 2013
Accepted 26 July 2013

Keywords:
Carbon nanotube
Molecular dynamics
Local buckling behavior
Stone–Wales defect
Vacancy defect

ABSTRACT

The local buckling behavior of perfect/defective and single/multi-walled carbon nanotubes (CNTs) under axial compressive forces has been investigated by the molecular dynamics approach. Effects of different types of defects including vacancy and Stone–Wales (SW) defects and their configurations on CNTs with different chiralities at room temperature are studied. Results show that defects largely reduce the buckling stress and the ratio of immediate reduction in buckling compressive stress of the defective CNT to the perfect one, but have little influence on their compressive elastic modulus. SW defects usually reduce the mechanical properties more than vacancy defects, and zigzag CNTs are more susceptible to defects than armchairs. In addition, increasing the number of defects leads to higher deterioration in mechanical properties of CNTs. The results of simulations show that in the case of slender single-walled CNTs, the behavior is primarily governed by the Euler buckling law. On the other hand, in the local shell buckling mode, two distinct behaviors are observed, including the primary local shell buckling mode for intermediate CNTs, and the secondary local shell buckling mode for short CNTs. In the local buckling response, CNTs with smaller diameters sustain higher buckling stresses than CNTs with larger diameters.

© 2013 Elsevier B.V. All rights reserved.

1. Introduction

Since their discovery in 1991 [1], carbon nanotubes (CNTs) have made a tremendous revolution in various industries due to their superior material properties, including high strength and low density. As a result, they are now being considered as an excellent alternative for conventional reinforcing fibers in structural composites and as a compressive component in nano-electro mechanical systems (NEMS).

Due to manufacturing restrictions, the possibility of production of perfect CNTs is much lower than the defective ones [2]. On the other hand, comparisons between the results of experimental and numerical simulation of CNTs confirm the fact that the theoretical and numerical predictions of mechanical properties of CNTs, such as the ultimate strength, are much higher than the experimental results. For example, the theoretical approaches [3,4] have reported that the CNT fracture strength is close to 100 GPa while the experimental results [5,6] indicate the fracture strength in the range of 11–63 GPa. The same pattern is observed for other mechanical properties such as the elastic modulus and the failure strain.

The discrepancy between the theory and experiment for the mechanical properties can be attributed to the fact that the existence of defects on the structure of CNTs is inevitable and they are susceptible to defects. In practice, it is almost impossible to find a CNT without any structural defects and imperfections, which are the likely causes of their low ultimate strength. Microscopic observations confirm that defects may be created at the stage of CNT growth and oxidation [7,8], purification processes (irradiation or oxidation) [9,10], chemical functionalization, or under mechanical strains.

Despite some drawbacks, defects have also shown advantages in some situations. For example, rehybridization defects increase the interfacial bonding strength between nanotubes and their surrounding matrix polymer [11] and facilitate the load transfer between different layers in multi-walled carbon nanotubes (MWCNTs) [12]. In addition, defects can be used as a hydrogen storage site in CNTs [13]. Furthermore, defects can also be useful in transition of nanotubes from one diameter to another, and on *Y* junction in molecular electronic [14]. Having realized potential advantages and drawbacks of defects, it is quite essential to consider their influence on the mechanical behavior of defective CNTs and CNT-reinforced composites.

On the other hand, CNTs may become mechanically unstable and buckle under compressive axial loads due to their high aspect ratio (length/diameter). Buckling can lead to failure in the form of a

* Corresponding author. Tel.: +98 21 6111 2258; fax: +98 21 6640 3808.
E-mail addresses: m.eftekhari@srbiau.ac.ir (M. Eftekhari), smoham@ut.ac.ir (S. Mohammadi), arkhoei@sharif.edu (A.R. Khoei).

0927-0256/$ - see front matter © 2013 Elsevier B.V. All rights reserved.
http://dx.doi.org/10.1016/j.commatsci.2013.07.034

sudden decline in the compressive load carrying capacity and undesirable distorted configuration of the structure. Therefore, the possibility of buckling should be considered seriously in devices which use CNT as a compressive component, such as composites, Atomic Force Microscopy (AFM) tip and hydrogen storages. Due to the fact that CNTs are highly prone to structural defects, investigation on mechanical stability and buckling of defective CNTs is inevitable.

In recent years, a few studies have been directed towards the buckling analysis of defective CNTs. For instance, the compressive behavior of single-walled carbon nanotubes (SWCNTs) in the presence of chemical functionalization and Stone–Wales (SW) defects was explored by Chandra and Namilae using Molecular dynamics (MD) simulations [15]. They found that functionalization and topological defects had a negative impact on buckling stresses of CNTs. The molecular mechanics (MM) approach was employed by Huq et al. [16] in order to explore the interaction of two neighboring SW defects and their influence on mechanical properties of SWCNTs under the axial compression. Their results indicated that at a certain distance, the interaction between two SW defects would vanish. In addition, it was revealed that zigzag SWCNTs with SW defects possessed higher buckling capacity than armchair counterparts. In addition, Hao et al. [2] found that vacancy defects heavily weakened the compressive load carrying capacity of CNTs and distinguished the density of the defects and their relative position as the main two factors which substantially influenced the buckling behavior of CNTs.

Investigation of the thermal buckling behavior of defective CNTs has shown that defects reduce the buckling capacities of defective SWCNTs and the degree of reduction depends on the type of defects, chirality and temperature. Simulations have revealed that point defects cause higher reduction in the buckling load than the SW defect [17]. Kulathunga et al. [18] studied the effects of various configurations of vacancy defects on buckling of SWCNTs in different thermal environments by MD simulation, and illustrated that increasing the number of vacancy defects significantly reduced the buckling stress of SWCNT. Ranjbartoreh and Wang [19] indicated that the axial stability of SWCNT decreased significantly due to topological defects and the critical buckling strain was more susceptible to defects than the critical buckling force. The slenderness ratio of defective CNTs on the buckling behavior was studied by Parvaneh et al. [20], who showed that single vacancy defects only had a weak influence on the critical buckling load of slender (length/diameter >12) CNTs at room temperature. In general, their results indicated that the effect of vacancy defects on buckling behavior were decreased by the increase of temperature.

After a comprehensive literature review, only a few number of investigations have been found on the buckling and postbuckling analysis of defective SWCNTs and MWCNTs with different chiralities and none of them have examined the effect of defects on the reduction of compressive stress after the buckling. Furthermore, the effect of different types of defects and their interaction on the local buckling analysis of SWCNTs and MWCNTs need to be comprehensively studied.

The main focus of this study is to investigate the effects of different types of defects on the local buckling and postbuckling behavior of SWCNTs and MWCNTs through a series of MD simulations. Different parameters such as the number of defects and their relative distance are considered. The stress–strain curves of defective and perfect CNTs under the uniaxial compression are determined, and the buckling stress, the compressive elastic modulus and the immediate reduction in buckling compressive stress of SWCNTs and MWCNTs are examined. In addition, the local buckling mode of SWCNTs with different tube diameters is compared with the Euler buckling theory.

2. Computational model

The structure of SWCNT is defined by a chiral vector (n,m). In the case of $n = m$, the CNT is called armchair and $m = 0$ makes a zigzag CNT. Two or more coaxial SWCNTs with an interlayer spacing of 0.34 nm form an MWCNT. Only double-wall CNTs are studied in this paper. The study is performed on two types of SWCNTs and MWCNTs. SWCNTs consist of a (10,10) armchair and a (17,0) zigzag containing 1660 and 1632 carbon atoms with diameters of 13.56 and 13.31 Å, respectively. The diameters are selected close to each other, but it is not possible to create any zigzag and armchair CNTs with exactly the same diameter. In addition, a (10,10)/(15,15) armchair (with 4100 carbon atoms and diameter of 20.34 Å) and a (17,0)/(26,0) zigzag (with 4128 carbon atoms and diameter of 20.35 Å) MWCNTs are also investigated. The lengths of all nanotubes are 100 Å.

Two forms of mechanical defects exist in nanotube structures, namely vacancy (Fig. 1a) and SW defects [21] (Fig. 1b) which is also known as 5–7–7–5 defect or twinned pentagon–heptagon pairs. The former defect can be formed by removing three convergent covalent bonds and an associated carbon atom from the nanotube structure (Fig. 1a), whereas the latter is a result of rotating a carbon–carbon bond by 90° with respect to its center to a new configuration, as shown in Fig. 1b. It is believed that the effects of defects remain relatively local and limited to the atoms at the vicinity of the defects.

The Tersoff interatomic potential function [22] is employed in order to describe the repulsive/attractive pair interaction among the carbon atoms. Further detail can be found in [22]. When CNTs are subjected to a tensile load, the original Tersoff potential predicts a sharp increase in the tensile fracture stress just prior to the rupture. This tensile fracture stress is several times larger than those predicted by the quantum mechanics (QM) [23]. In order to avoid such a nonphysical failure mechanism in the tensile models, the smooth cut-off function is replaced by a rigid cut-off distance and the cut-off radius is extended from 1.7 to 2 Å. Such a modified cut-off distance prevents artificial stiffening and nonphysical fracture behavior of CNTs (Fig. 2). This modified version of potential is not capable of handling bond formation mechanisms.

Modification of the original Tersoff potential is not necessary in compressive analysis due to the fact that most of carbon bonds are only subjected to compressive forces and even if some of covalent bonds fell into the tensile region, their elongation would not go beyond R_{ij}, so modifying the cut-off function does not significantly affect the overall compressive behavior (Fig. 3).

The long-range non-bonded interaction between carbon atoms in different layers of MWCNTs is described by the Lenard–Jones (LJ) 6–12 potential. For carbon atoms, these parameters are $\varepsilon_{C-C} = 0.00239$ eV and $\sigma_{C-C} = 0.34$ nm [24]. The effect of the van der Waals force can be neglected for distances larger than $2.5\sigma = 0.85$ nm. The LAMMPS (Large-scale atomic/molecular massively parallel simulator) open source code [25], is employed to carry out the MD simulation of the buckling behavior of CNTs. The VMD (Visual Molecular Dynamics) open source code software is used for the visualization purposes [26].

MD simulations are performed to investigate the buckling behavior of CNTs. At the first stage of simulation, the structure of CNT is relaxed to the room temperature (300 K) by adopting the so-called constant Number of atoms, Volume and Temperature ensemble (NVT ensemble) in 20,000 steps. A random velocity is applied to all atoms in order to reach the specified temperature. Afterwards, the energy minimization procedure is carried out by the conjugate gradient (CG) algorithm in order to remove the existing residual stresses of CNT before beginning the simulation of compression phase.

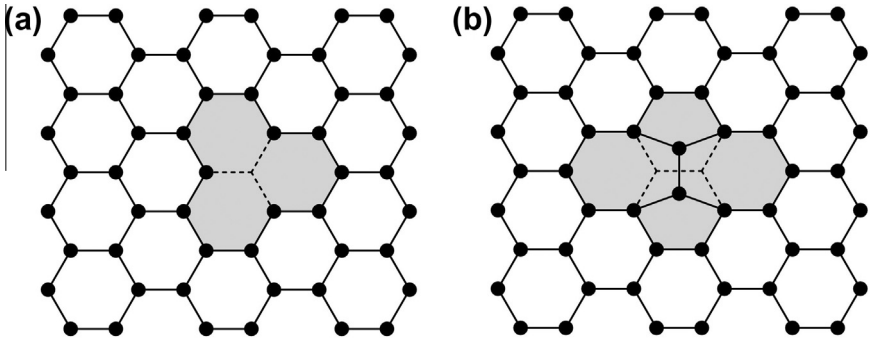

Fig. 1. Two types of topological defects in CNTs: (a) vacancy defect and (b) SW defect.

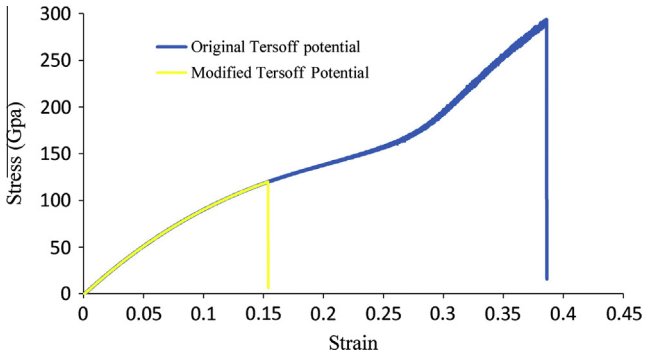

Fig. 2. Stress–strain curve of SWCNT under the tensile loading.

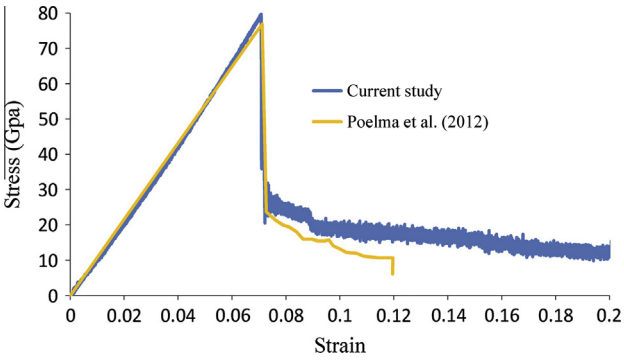

Fig. 4. Force-strain curve for (10,0) zigzag in compression.

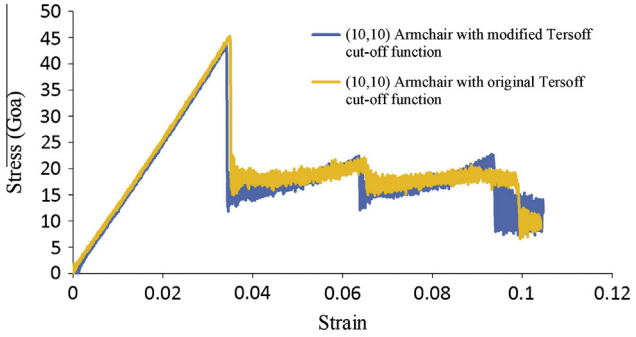

Fig. 3. Compressive stress–strain curve for the perfect (10,10) armchair nanotube with original and modified Tersoff cut-off functions.

After the system reaches the equilibrium state, buckling simulations can be performed. The axial compression is applied by moving downwards the atoms at the top with the constant velocity of 0.01 Å/fs, while the atoms at the bottom are fixed. The time integration step is set to 1 fs. A total of 1,000,000 time steps are used to simulate the whole buckling response of CNTs.

3. Results and discussions

In order to verify the buckling analysis, a perfect (10,0) zigzag SWCNT, previously modeled by Poelma et al. [27] based on the Dreiding forcefield [28], is considered. The length and diameter of SWCNT are 52.62 and 7.83 Å, respectively, and the model is fixed at the two ends. The simulation is performed at the room temperature (300 K). According to Fig. 4, a good agreement is clearly observed with the reference results.

The results of simulations are organized into two main parts. The first part discusses the buckling behavior of defective SWCNTs, and the second part is mainly focused on the influence of defects on the buckling behavior of MWCNTs.

3.1. Effect of angle between defects on buckling of SWCNT

The axial strain of CNT is computed as $\varepsilon = |\Delta L/L_0|$, where L_0 is the initial length and ΔL is the compressive deformation of CNT. The axial stress of SWCNT is obtained by $\sigma_{SWCNT} = F/A_{SWCNT}$, where $A_{SWCNT} = \pi D t$, F is the axial force, D is the tube diameter, and t is the wall thickness. Several authors have recently used the interlayer spacing in graphite (0.34 nm) as the thickness of CNT [2,15,27,29–36], so this value is chosen for the thickness of CNT. An important point, however, is that the thickness of CNT does not affect the performed MD simulations and the obtained MD solutions. Nevertheless, it may affect the post processing procedures such as evaluation of the system pressure and subsequently the compressive stress. Most of the results in this paper are the relative values. As a result, the change in the thickness of CNT does not affect them. For example the ratio, defined in (1), does not depend on the cross section and the thickness of the CNT.

$$\frac{\sigma_{Defective}}{\sigma_{Perfect}} = \frac{F_{Defective}/A}{F_{Perfect}/A} = \frac{F_{Defective}}{F_{Perfect}} \tag{1}$$

The buckling stress–strain curve for the perfect SWCNT under axial compression is depicted in Fig. 5. The maximum compressive stress for the perfect SWCNT increases almost linearly as the tube is further strained in compression step by step before it buckles abruptly. It should be noted that the Young's modulus (E) is defined as the initial tangent modulus at zero strain.

Based on the result of Hao et al. [2], there are at least two main influencing effects of the defect on the mechanical properties of CNTs; the total number of defects and their relative position (Fig. 6). Both vacancies and SW defects, which are located in the

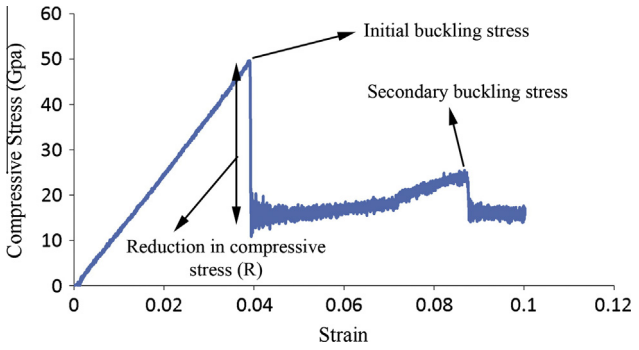

Fig. 5. Typical stress–strain curve for SWCNT in compression.

Table 1
Variation of $\sigma_{Defective}/\sigma_{Perfect}$ for (10,10) armchair and (17,0) zigzag SWCNTs with vacancy and SW defects.

Armchair(10)			Zigzag(17)		
Angle (°)	Vacancy	SW	Angle (°)	Vacancy	SW
36	0.79	0.69	21	0.62	–
72	0.80	0.74	42	0.79	0.55
108	0.87	0.68	64	0.76	0.56
144	0.86	0.78	85	0.77	0.46
180	0.89	0.75	106	0.82	0.47
			127	0.87	0.58
			148	0.81	0.61
			169	0.86	0.60

mid-length of SWCNT, are studied. These defects are located in different angles with respect to each other and the effect of this angle on different mechanical properties such as the buckling stress and the compressive elastic modulus are examined. Then, multiple numbers of defects (both vacancy and SW) are located on circumferences of SWCNT with equal relative angles to investigate their influence on the same mechanical properties.

The buckling stress for the perfect (10,10) armchair and (17,10) zigzag SWCNTs are 43.55 and 45.4 GPa, respectively. Table 1 represents the ratio of buckling stress of defective SWCNT to the perfect one ($\sigma_{Defective}/\sigma_{Perfect}$) with respect to the angle between two defects. It is worth-mentioning that the effect of vacancy defect on buckling stress of zigzag SWCNT is more than the armchair one. A number of important conclusions can be made by comparing the influence of SW and vacancy defects on armchair and zigzag SWCNTs, as depicted in Table 1. Firstly, SW defects always decrease the buckling stress more than vacancies in both types of SWCNTs. Secondly, SW defects show more influence on zigzag SWCNTs than the armchairs, and reduce the buckling stress more significantly (54% reduction).

An important point about the SW formation in zigzag nanotubes is that when two SW defects are formed in two adjacent bonds, the distance between the two carbon atoms, which are located on rotated bonds, is reduced from 1.42 to 1.05 Å. This reduction causes a significant increase in the interaction force between the two atoms and so the governing MD equations may diverge. As a result, formation of two SW defects in adjacent bonds seems practically impossible (Fig. 7).

The results of present simulations indicate that the elastic modules for perfect (10,10) armchair and (17,0) zigzag SWCNT are 1280.8 and 1283.6 GPa, respectively. Variation of elastic modulus ratio of defective SWCNT to the perfect one ($E_{Defective}/E_{Perfect}$) with respect to the angle between the two defects are reported in Table 2. The results lead to the point that the existence of SW defects in both types of SWCNTs always decreases the elastic modulus more than the vacancy defects. However, this reduction for zigzag SWCNT with the SW defect is much more than the armchair one, where a maximum 16% reduction is observed in $E_{Defective}/E_{Perfect}$. Such a significant amount of degradation does not occur in other models.

Most of simulations have resulted in a similar trend and the overall behavior of buckling stress–strain curve comprises of a rise in the stress–strain curve with a constant rate and then, at the buckling point, the stress suddenly falls down, accompanied with occurrence of a significant geometrical deformation in the middle section. Afterwards, the nanotube partially recovers its geometric stiffness and the process of increasing stress continues with a much lower pace.

Denoting R as the immediate reduction in the buckling compressive stress (as depicted in Fig. 5), the ratio of R of the defective to the perfect nanotube can be defined as:

$$R_{DP} = R_{Defective}/R_{Perfect} \tag{2}$$

Table 3 shows the variation of R_{DP} with respect to the angle between defects. Accordingly, in all cases, a perfect SWCNT shows more immediate reduction in the buckling compressive stress than the same defective SWCNT for both SW and vacancy defects. This is due to the fact that the perfect tube in the buckling instant bears more compressive stress than the defective one. Consequently, such compressive forces make bigger distortive out of plane deformation in the perfect tube, which leads to the phenomenon that the nanotube structure shows more instability, with occurrence of higher stress reduction. According to Table 3, R_{DP} for the armchair SWCNT with SW defects is higher than the zigzag one. In addition, SWCNTs with vacancy defects show higher R_{DP} than nanotubes with SW. This can be attributed to the fact that the

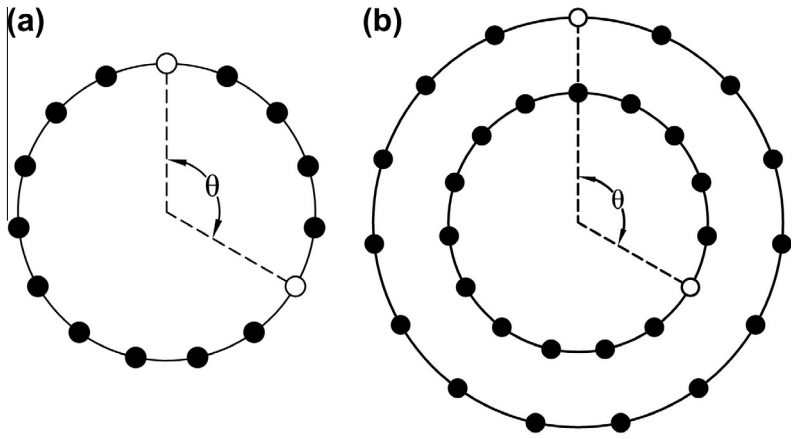

Fig. 6. Angle between two defects (either vacancy or SW) in a) SWCNTs and b) MWCNTs.

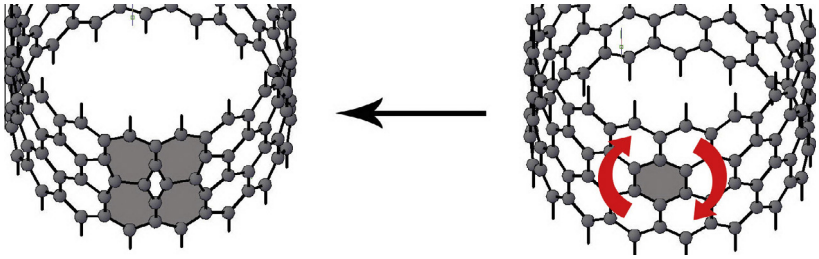

Fig. 7. Formation of two SW defects in two adjacent bonds.

Table 2
Variation of $E_{Defective}/E_{Perfect}$ for (10,10) armchair and (17,0) zigzag with vacancy and SW defects.

Armchair(10)			Zigzag(17)		
Angle (°)	Vacancy	SW	Angle (°)	Vacancy	SW
	$E_{Defective}/E_{Perfect}$			$E_{Defective}/E_{Perfect}$	
36	0.976	0.954	21	0.950	–
72	0.978	0.951	42	0.968	0.932
108	0.980	0.953	64	0.969	0.882
144	0.982	0.959	85	0.975	0.839
180	0.979	0.958	106	0.978	0.941
			127	0.979	0.931
			148	0.976	0.927
			169	0.980	0.923

Table 3
Variation of R_{DP} for (10,10) armchair and (17,0) zigzag with vacancy and SW defects.

Armchair(10)			Zigzag(17)		
Angle (°)	Vacancy	SW	Angle (°)	Vacancy	SW
	$E_{Defective}/E_{Perfect}$			$E_{Defective}/E_{Perfect}$	
36	0.46	0.29	21	0.35	
72	0.67	0.52	42	0.57	0.20
108	0.72	0.26	64	0.41	0.32
144	0.75	0.60	85	0.57	0.14
180	0.81	0.61	106	0.73	0.13
			127	0.75	0.31
			148	0.57	0.37
			169	0.74	0.38

bonds between the carbon atoms in SWCNT with SW defects already exist and they can help the overall structure of nanotube to maintain its stability to some extent after the buckling point, while in a vacancy defect, the three covalent bonds connected to a missing carbon atom are completely removed.

3.2. Effect of number of defects in SWCNTs

The next step is to investigate the effect of number of defects on buckling and post-buckling stress of SWCNTs. In this regard, a number of 2–10 defects (both vacancy and SW) with equal angles, are located on circumferences of (10,10) armchair and (17,0) zigzag SWCNTs, as depicted in Fig. 8.

Fig. 9 indicates that when the number of vacancy defects in the middle section of the armchair SWCNT increases, its buckling stress reduces. A more severe degradation in the buckling stress up to 48% is observed in the armchair with vacancy defect. The existence of SW defects in the zigzag SWCNT causes more reduction in the buckling stress than the armchair one up to 57%. Fig. 9 also illustrates that in contrast to the effect of vacancy defect, increasing the number of SW defects in both types of SWCNTs, results in convergence of $\sigma_{Defective}/\sigma_{Perfect}$ towards a constant value. In other word, increasing the number of SW defects after a certain number does not affect the buckling behavior. SW defects always cause higher decrease in $\sigma_{Defective}/\sigma_{Perfect}$ ratio in zigzag SWCNT than vacancies, but this is not the case in armchair SWCNT, where by the increase of the number of SW defects from a certain number, vacancy defects could be more critical.

Another observation is that during the relaxation phase towards 300 K temperature of armchair and zigzag SWCNTs with large number of SW defects, out of plane distortion occurs in the cross section of SW defects. This distortion for armchair SWCNT is towards the inside of the cylinder, while for the zigzag SWCNT is outwards, as depicted in Fig. 10. In contrast, due to the fact that vacancy defects do not distort the cylindrical structure of nanotube, the overall buckling behavior of nanotubes with vacancy defects remains the same.

The influence of SW defects on the elastic modulus of both SWCNTs is far higher than the vacancy defects. In addition, while equal number of SW defects on the zigzag SWCNT reduces the elastic modulus more than the armchair one, the effect of vacancy defects on both types remains relatively identical (Fig. 11).

Fig. 12 illustrates that the effect of vacancy defects on R_{DP} in both types of SWCNTs is almost the same, and when the number of vacancies increases, R_{DP} is decreased. On the contrary, while the number of SW defects in a section of SWCNT increases, the value of R_{DP} is limited to a specific value, indicating that it does not affect R_{DP} after a certain number of defects. Also, it is worth mentioning that the existence of SW defects results in much lower R_{DP} in zigzag SWCNTs than armchairs with SW defects.

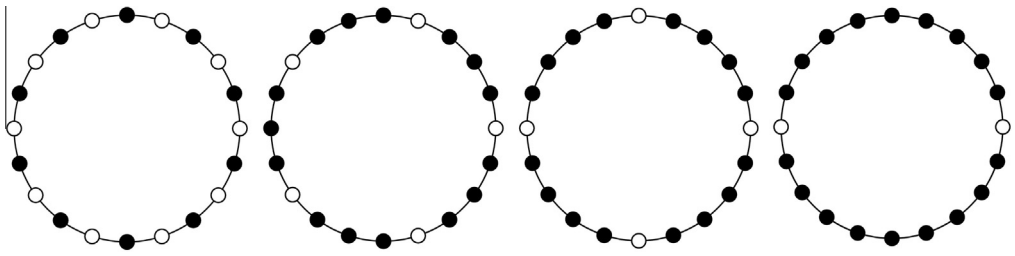

Fig. 8. Equal distribution of defects (either vacancy or SW) on SWCNT.

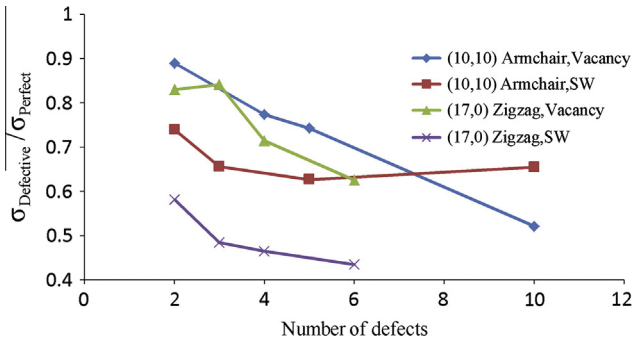

Fig. 9. Variation of $\sigma_{Defective}/\sigma_{Perfect}$ for (10,10) armchair and (17,0) zigzag with vacancy and SW defects.

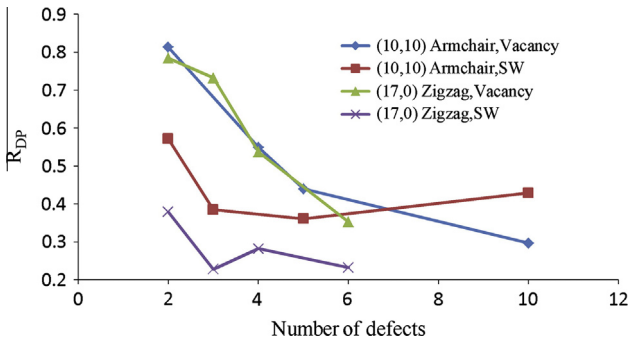

Fig. 12. Variation of R_{DP} for (10,10) armchair and (17,0) zigzag with vacancy and SW defects.

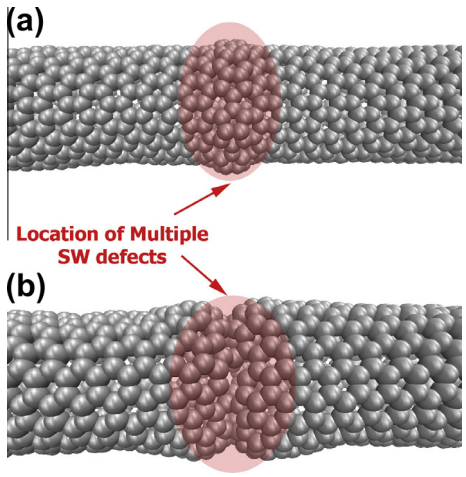

Fig. 10. Distortion in SWCNT with multiple SW defects. Large out-of-plane deformations occur in the cross section of SW defects: (a) (10,10) armchair with 10 SW defects and (b) (17,0) zigzag with 6 SW defects.

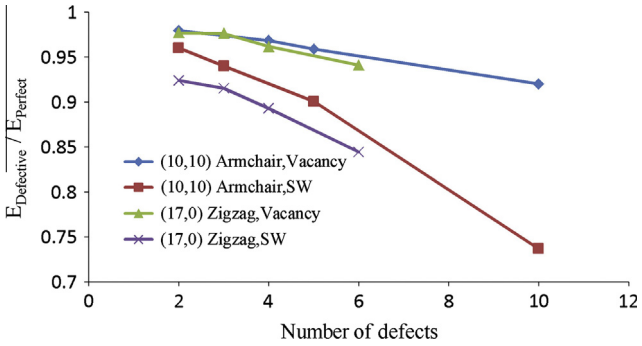

Fig. 11. Variation of $E_{Defective}/E_{Perfect}$ for (10,10) armchair and (17,0) zigzag with vacancy and SW defects.

3.3. Effect of angle between defects in MWCNT

Two defects are considered for MWCNTs; one on the inner tube and the other on the outer tube. Then, the effect of the angle between the two defects on mechanical properties is investigated (see Fig. 6b). The stress can be calculated by $\sigma_{MWCNT} = F/A_{MWCNT}$, where A_{MWCNT} is the area of the cross section of MWCNT,

$$A_{MWCNT} = \pi(r_{out} + t/2)^2 - \pi(r_{in} - t/2)^2 \quad (3)$$

where r_{in} and r_{out} are the radii of the inner and outer tubes, respectively.

During the compressive loading, the MWCNT loses its cylindrical shape both on the middle section where the defect exists and on one of the sides (Fig. 13a). Afterwards, the same process is almost repeated on the other side of MWCNT (Fig. 13b). At last, the MWCNT loses its axial stiffness and undergoes eccentric deformation, as depicted in Fig. 13c.

An interesting observation in buckling analysis of MWCNT is that the inner and outer tubes buckle concurrently. At the first glance and based on the basic engineering rules, it seems that the outer tube must be stronger than the inner one (because of smaller ratio of L/D of the outer tube). In order to examine which tube buckles sooner, two (10,10) and (15,15) armchair SWCNTs are analyzed under the compressive loading. Surprisingly, the (10,10) armchair, which is slender, bears more compressive stress (45 GPa) than the (15,15) armchair with 28 GPa compressive stress (Fig. 14). Clearly, this cannot be justified based on the conventional theories of mechanics of materials. The reason is attributed to the fact that occurrence of local buckling dominates the global behavior of SWCNTs. When the diameter of SWCNT increases, the behavior of the specimen changes from a global bending beam model to local out of plane shell mode, where the model becomes more susceptible to the local buckling.

In practice, when two individual tubes comprise an MWCNT, both of them buckle concurrently. The reason can be attributed to the fact that when the outer tube is going to buckle, the van der Waals interaction between the inner tube and the outer one

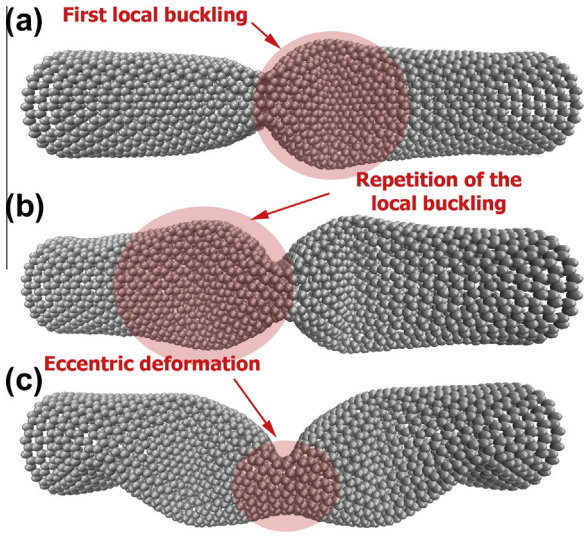

Fig. 13. Typical local buckling progress in an MWCNT: (a) occurrence of the local buckling; (b) repetition of the local buckling on the other side and (c) eccentric deformation.

imposes out of plane forces on the outer tube and prevents occurrence of buckling in the outer one. This remains to be effective until the inner tube reaches its ultimate buckling stress and at this moment both tubes lose their axial stiffness and buckle almost concurrently (Fig. 15). As a result, the buckling stress of MWCNTs is mainly governed by the size of the innermost tube.

In order to further clarify the fact that nanotubes with more slenderness ratio may buckle at higher stress levels, three (7,7), (10,10) and (13,13) armchair SWCNTs with different lengths are modeled. Fig. 16 shows that when SWCNTs with different length to diameter ratios (L/D) are subjected to compressive loading, the following distinct behaviors are observed (Fig. 16):

(i). For L/D ratios greater than around 21 and in the case of slender SWCNTs, there is practically no significant difference in the buckling stress for different diameters and the behavior is primarily governed by the global Euler buckling principle.
(ii). If L/D ratio is smaller than 21, the Euler buckling behavior of SWCNTs is changed into the local shell buckling mode. In this region two distinct behaviors can be recognized:
(a) Primary local shell buckling mode for intermediate CNTs,
(b) Secondary local shell buckling mode for short CNTs. In this case, the buckling stress rises with a sharper trend, because the energy required for activation of the secondary mode is always greater than the primary one.

In the local shell buckling region, CNTs with smaller diameters sustain higher buckling stress than CNTs with larger diameters. Based on the knowledge of the authors, no published report is available on such a phenomenon yet.

For analytical calculation of the Euler buckling stress, it is assumed that the average compressive Young's modulus of SWCNT is 1250 GPa. Therefore, if the SWCNT behaves similar to an elastic circular cylindrical column, its Euler buckling stress can then be obtained from:

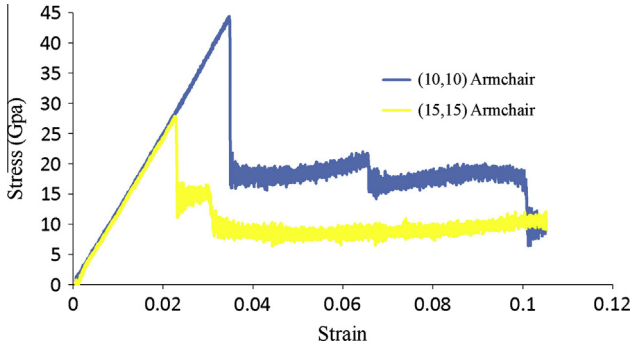

Fig. 14. Buckling behavior in (10,10) and (15,15) armchair SWCNTs.

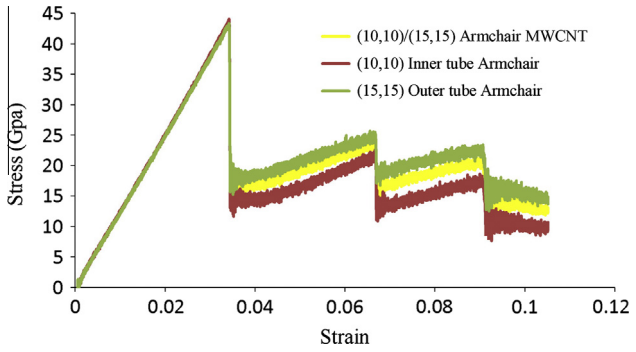

Fig. 15. Buckling behavior in (10,10)/(15,15) armchair MWCNT.

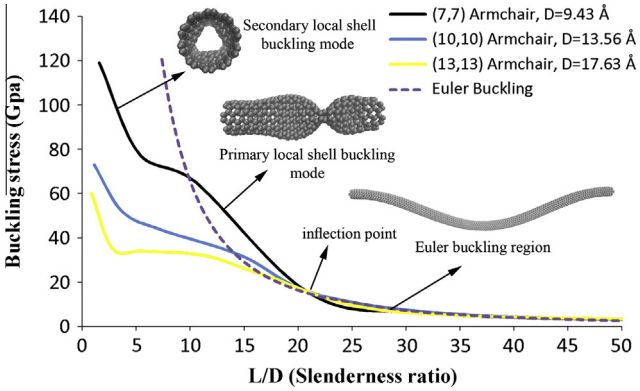

Fig. 16. Buckling analysis of armchair SWCNTs with different slenderness ratios.

$$\sigma_{Euler} = \frac{\pi^2 \times E}{(kL/r_{gyr})^2} \tag{4}$$

with

$$r_{gyr} = \sqrt{\frac{I_{SWCNT}}{A_{SWCNT}}} \tag{5}$$

$$I_{SWCNT} = \frac{\pi \times ((D+t)^4 - (D-t)^4)}{64} \tag{6}$$

where L is the length of nanotube, r_{gyr} is the radius of gyration and I_{SWCNT} is assumed to be the moment of inertia of the nanotube section. The effective length factor for the fixed–fixed SWCNT is assumed to be $k = 0.5$ (the nanotube is modeled as a two-fixed end column).

The buckling stress for the perfect (10,10)/(15,15) armchair and (17,0)/(26,0) zigzag MWCNTs with length of 100 Å are 43.35 and 40.38 GPa, respectively. Based on the results of Figs. 17 and 18, it is observed that the SW defects reduce mechanical properties (elastic modulus and buckling stress) of both types of MWCNTs more than the vacancy ones. The most reduction in the buckling stress is observed in zigzag MWCNTs with SW defect at about 35% strength degradation. R_{DP} in both types of MWCNTs with vacancy defect is higher than the SW one (Fig. 19). It is clearly observed that, R_{DP} is always less than unity. As expected, the compressive elastic modulus is not largely affected by the existence of defect in MWCNTs and the reduction is negligible (Fig. 18). Also, this decrease in the elastic modulus for inner tube is more than the outer one.

3.4. Effect of number of defects in MWCNT

In the next step, the effect of number of vacancy and SW defects on buckling and post-buckling stresses of (10,10)/(15,15) armchair and (17,0)/(26,0) zigzag MWCNTs is investigated. Various number of defects (both vacancy and SW) are located on the circumference of inner and outer tubes with equal angles (see Fig. 20).

In contrast to the result of SWCNTs with multiple defects (Fig. 9), which the buckling stress ratio for armchair SWCNT with vacancy defect is more than the zigzag one, in the case of MWCNT, the buckling stress ratio for the armchair MWCNT is lower than the zigzag one (Fig. 21). The most reduction, which is observed in zigzag MWCNT with SW defect, is about 50%. Similar to the results of SWCNT with multiple defects, the buckling stress for both types of MWCNT is more sensitive to the existence of SW defects than the vacancy one.

Although the effect of existence of multiple vacancy defects on the compressive elastic modulus of both types of MWCNTs are the same, but in the case of multiple SW defects, the difference is

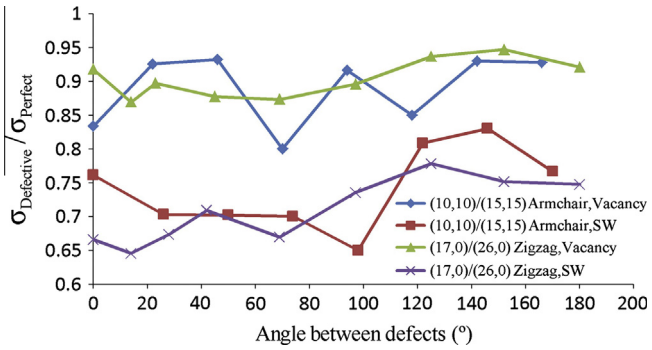

Fig. 17. Variation of $\sigma_{Defective}/\sigma_{Perfect}$ for (10,10)/(15,15) armchair and (17,0)/(26,0) zigzag MWCNTs with vacancy and SW defects.

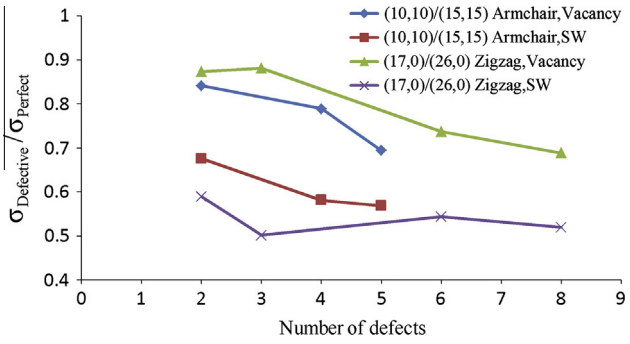

Fig. 21. Variation of $\sigma_{Defective}/\sigma_{Perfect}$ for (10,10)/(15,15) armchair and (17,0)/(26,0) zigzag MWCNTs with multiple vacancy and SW defects.

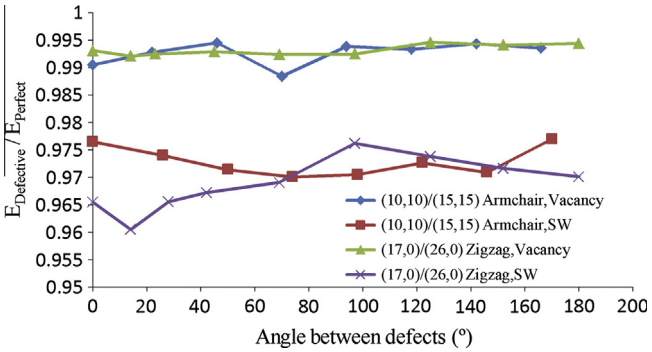

Fig. 18. Variation of $E_{Defective}/E_{Perfect}$ for (10,10)/(15,15) armchair and (17,0)/(26,0) zigzag MWCNTs with vacancy and SW defects.

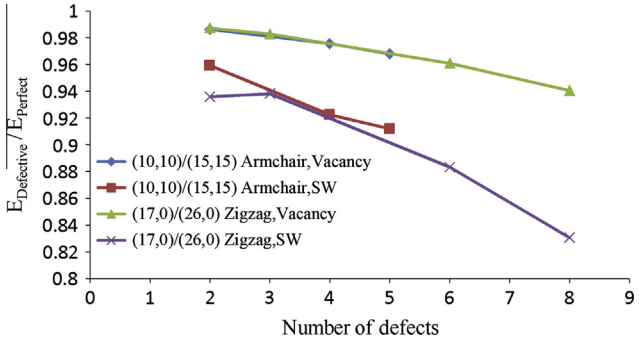

Fig. 22. Variation of $E_{Defective}/E_{Perfect}$ for (10,10)/(15,15) armchair and (17,0)/(26,0) zigzag MWCNTs with multiple vacancy and SW defects.

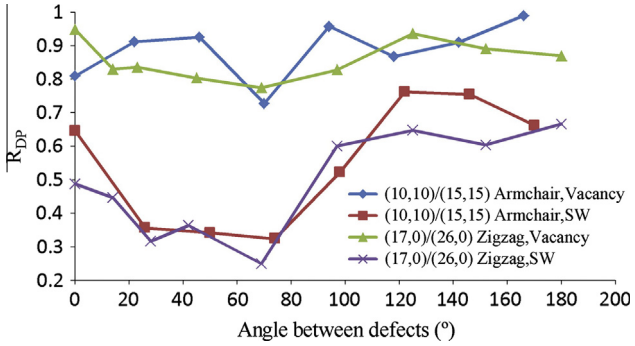

Fig. 19. Variation of R_{DP} for (10,10)/(15,15) armchair and (17,0)/(26,0) zigzag MWCNTs with vacancy and SW defects.

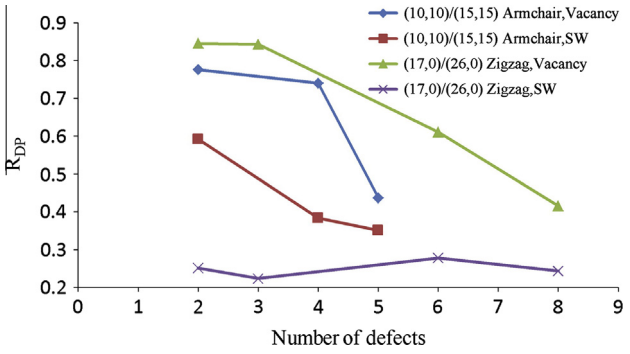

Fig. 23. Variation of R_{DP} for (10,10)/(15,15) armchair and (17,0)/(26,0) zigzag MWCNTs with multiple vacancy and SW defects.

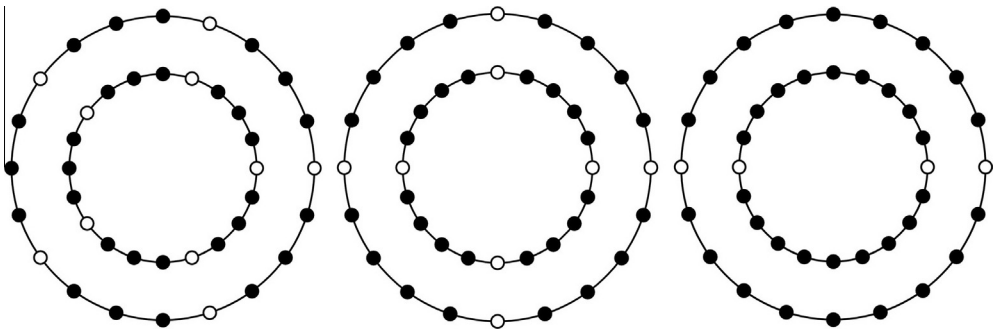

Fig. 20. Uniform distributions of defects (either vacancy or SW) on MWCNTs.

negligible. In addition, SW defects largely reduce the elastic modulus of MWCNT up to 17% (Fig. 22).

Finally, Fig. 23 illustrates that R_{DP} for MWCNT with multiple SW defects is less than the vacancy defects and this parameter for zigzag MWCNTs with SW defects is minimum. These results prove that R_{DP} in both types of SWCNTs and MWCNTs is always less than unity.

4. Conclusion

The local buckling behavior of perfect and defective SWCNTs and MWCNTs under uniaxial compression has been studied by a series of MD simulations. The findings of the present study have provided further in-depth understanding of the compressive behavior of CNTs, which are frequently used as a compressive component in composites and nanomechanical devices.

It has been observed that the defects largely reduce the buckling stress and the ratio of immediate reduction in buckling compressive stress of the defective to the perfect nanotube (R_{DP}) of CNTs, but have little influence on their elastic modulus. Results show that in most cases, the effect of vacancy and SW defects on the buckling stress and elastic modulus of zigzag CNT is more than the armchair one. In addition, SW defects usually show more influence on the buckling stress and elastic modulus for both types of CNTs than the vacancy ones.

When two individual tubes comprise an MWCNT, both of them buckle concurrently due to the existence of van der Waals interaction between the inner and outer tubes. It means that the buckling stress of MWCNTs is dominated by the size of the innermost tube. The behavior is primarily governed by the Euler buckling for slender CNTs. On the other hand, in the local shell buckling mode, CNTs with smaller diameters sustain higher buckling stress than CNTs with larger diameters.

Acknowledgements

The authors would like to acknowledge the financial support of Iran Nanotechnology Initiative Council under the grant no. 46702. Also the support of Iran National Science Foundation is gratefully appreciated.

References

[1] S. Iijima, Nature 354 (1991) 56–58.
[2] X. Hao, H. Qiang, Y. Xiaohu, Compos. Sci. Technol. 68 (2008) 1809–1814.
[3] D. Qian, G.J. Wagner, W.K. Liu, M.-F. Yu, R.S. Ruoff, Appl. Mech. Rev. 55 (2002) 495–533.
[4] L. Qiang, B. Baidurya, Nanotechnology 16 (2005) 555–566.
[5] M.-F. Yu, O. Lourie, M.J. Dyer, K. Moloni, T.F. Kelly, R.S. Ruoff, Science 287 (2000) 637–640.
[6] M. Sammalkorpi, A. Krasheninnikov, A. Kuronen, K. Nordlund, K. Kaski, Phys. Rev. B 70 (2004) 245416.
[7] D.B. Mawhinney, V. Naumenko, A. Kuznetsova, J.T. Yates Jr, J. Liu, R.E. Smalley, Chem. Phys. Lett. 324 (2000) 213–216.
[8] R. Andrews, D. Jacques, D. Qian, E.C. Dickey, Carbon 39 (2001) 1681–1687.
[9] A.V. Krasheninnikov, K. Nordlund, J. Vac. Sci. Technol., B 20 (2002) 728–733.
[10] S.L. Mielke, D. Troya, S. Zhang, J.-L. Li, S. Xiao, R. Car, R.S. Ruoff, G.C. Schatz, T. Belytschko, Chem. Phys. Lett. 390 (2004) 413–420.
[11] Z.H. Xia, P.R. Guduru, W.A. Curtin, Phys. Rev. Lett. 98 (2007) 245501.
[12] M. Huhtala, A.V. Krasheninnikov, J. Aittoniemi, S.J. Stuart, K. Nordlund, K. Kaski, Phys. Rev. B 70 (2004) 045404.
[13] T. Kondo, K. Shindo, M. Arakawa, Y. Sakurai, J. Alloy. Compd. 375 (2004) 283–291.
[14] Z. Yao, H.W.C. Postma, L. Balents, C. Dekker, Nature 402 (1999) 273–276.
[15] N. Chandra, S. Namilae, Mech. Adv. Mater. Struct. 13 (2006) 115–127.
[16] A.M.A. Huq, K.L. Goh, Z.R. Zhou, K. Liao, J. Appl. Phys. 103 (2008) 054306–054307.
[17] Y.Y. Zhang, Y. Xiang, C.M. Wang, J. Appl. Phys. 106 (2009) 113503–113508.
[18] D.D.T.K. Kulathunga, K.K. Ang, J.N. Reddy, J. Phys.: Condens. Mater. 22 (2010) 345301.
[19] A. Ranjbartoreh, G. Wang, Nanoscale Res. Lett. 6 (2011) 28.
[20] V. Parvaneh, M. Shariati, A.M. Majd Sabeti, Eur. J. Mech. A – Solid 28 (2009) 1072–1078.
[21] A.J. Stone, D.J. Wales, Chem. Phys. Lett. 128 (1986) 501–503.
[22] J. Tersoff, Phys. Rev. B 39 (1989) 5566–5568.
[23] S. Zhang, S.L. Mielke, R. Khare, D. Troya, R.S. Ruoff, G.C. Schatz, T. Belytschko, Phys. Rev. B 71 (2005) 115403.
[24] J. Xiao, B. Liu, Y. Huang, J. Zuo, K.C. Hwang, M.F. Yu, Nanotechnology 18 (2007) 395703.
[25] S. Plimpton, J. Comput. Phys. 117 (1995) 1–19.
[26] W. Humphrey, A. Dalke, K. Schulten, J. Mol. Graphics 14 (1996) 33–38.
[27] R.H. Poelma, H. Sadeghian, S. Koh, G.Q. Zhang, Microelectron. Reliab. 52 (2012) 1279–1284.
[28] S.L. Mayo, B.D. Olafson, W.A. Goddard, J. Phys. Chem. 94 (1990) 8897–8909.
[29] S.L. Mielke, S. Zhang, R. Khare, R.S. Ruoff, T. Belytschko, G.C. Schatz, Chem. Phys. Lett. 446 (2007) 128–132.
[30] L. Pan, Z. Shen, Y. Jia, X. Dai, Physica B 407 (2012) 2763–2767.
[31] R. Khare, S.L. Mielke, J.T. Paci, S. Zhang, R. Ballarini, G.C. Schatz, T. Belytschko, Phys. Rev. B 75 (2007) 075412.
[32] N.M. Pugno, J.A. Elliott, Physica E 44 (2012) 944–948.
[33] Y. Kuang, S.Q. Shi, P.K. Chan, C.Y. Chen, Nanotechnology 21 (2010) 6.
[34] H. Song, X. Zha, Physica B 403 (2008) 3798–3802.
[35] Z. Qin, Q.-H. Qin, X.-Q. Feng, Phys. Lett. A 372 (2008) 6661–6666.
[36] N. Hu, K. Nunoya, D. Pan, T. Okabe, H. Fukunaga, Int. J. Solids Struct. 44 (2007) 6535–6550.